Molecular Dynamics Study of the IIA Binding Site in Human Serum Albumin: Influence of the Protonation State of Lys195 and Lys199

Natalia Díaz,[†] Dimas Suárez,[‡,#] Tomás L. Sordo,[†] and Kenneth M. Merz, Jr.*[,‡]

Departamento de Química Física y Analítica, Universidad de Oviedo, C/Julián Clavería 8, 33006 Oviedo, Asturias, Spain, and Department of Chemistry, Eberly College of Sciences, The Pennsylvania State University, 152 Davey Laboratory, University Park, Pennsylvania 16802-6300

Received August 7, 2000

The IIA binding site of human serum albumin (HSA) preferentially binds hydrophobic organic anions of medium size (e.g., aspirin, benzylpenicillin, warfarin, etc.) and bilirubin. This binding ability is particularly important for the distribution, metabolism, and efficacy of drugs. In addition, HSA can also covalently link to different IIA substrates owing to the presence of a highly reactive residue, Lys199, which is strategically located in the IIA site. Herein, we present results of three restrained molecular dynamics (MD) simulations of the IIA binding site on the HSA protein. From these simulations, we have determined the influence that the ionization state of the key residue, Lys199, and the nearby Lys195 has on the structure and dynamics of the IIA binding site. When Lys199 is neutral the computed average distances for the most significant interresidue contacts are in good agreement with those estimated from the X-ray coordinates. The analysis of the solvent structure and dynamics indicates that the basic form of Lys199 is likely connected to the acid form of Lys195 through a network of H-bonding water molecules with a donor → acceptor character. The presence of these water bridges can be important for stabilizing the configuration of the IIA binding site and/or promoting a potential Lys195 → Lys199 proton-transfer process. These results suggest that both lysine residues located in the IIA binding site of HSA, Lys195 and Lys199, could play a combined and comparable chemical role. Our simulations also give insight into the binding of bilirubin to HSA.

Introduction

Human serum albumin (HSA) constitutes ∼60% of the mass of plasma protein with a typical concentration of 5 g/100 mL in the circulatory system. Because of its availability, stability, and ligand binding ability, the metabolism and genetics of HSA have been extensively studied for many years using a broad range of experimental techniques.[1,2] HSA is unique because of its myriad of functions: the most important role of HSA is its transport and delivery functions in the bloodstream thanks to its exceptional ability to bind reversibly a large variety of ligands. Remarkably, the abundance of HSA and its carrier function are also crucial for the distribution, metabolism, and efficacy of small-compound drugs which are bound to HSA. In addition, albumin accounts for 80% of the colloid osmotic pressure of plasma, plays an important role in maintaining the pH of extravascular fluids, and is of significance as a protective agent, as a factor in lipid metabolism, and in other miscellaneous functions.

The HSA consists of 585 amino acids and has a molecular mass of 65 kDa. Its amino acid sequence is characterized by a large percentage of cysteine residues (6%). These residues, except one, are involved in 17 disulfide linkages, which are important in stabilizing the HSA structure. HSA also contains a large number of charged amino acids (31%). Curiously, there is only one tryptophan residue in the protein, which has been particularly advantageous in binding experiments with fluorescence probes.[1] The three-dimensional structure of HSA remained largely unknown until the first crystal structure of HSA at 2.8 Å resolution was reported in 1992.[3] Since then several independent X-ray structural determinations of HSA to a resolution of 2.5 Å have been published.[4,5] According to these X-ray analyses, the HSA molecule has a high α-helical content (67%) and is a heart-shaped molecule 80 Å on a side, with an average thickness of 30 Å (see Figure 1). The tertiary structure of HSA is composed of three repeating domains: domain I (residues 1−197), domain II (residues 189−385), and domain III (residues 381−585), which are characterized by a common motif of 10 α-helices. Each domain is divided into two subdomains (A, B) where the helices h1−h4 in subdomain A are homologous to h7−h10 in subdomain B. The partially overlapping regions of the domains are a consequence of the helical continuation from the C-terminal portion of the IB and IIB helices to the N-terminal helices of IIA and IIIA (helices: $h10_I$−$h1_{II}$ and $h10_{II}$−$h1_{III}$), respectively.[6]

Albumin interacts with a broad spectrum of compounds thanks to its three-domain design which provides a variety of binding sites.[1,7] Most strongly bound are hydrophobic organic anions of medium size, long-chain fatty acids, and bilirubin. For small negatively charged ligands (warfarin, aspirin, diazepam, ibuprofen, benzylpenicillin, triodobenzoate, etc.), previous studies

* To whom correspondence should be addressed. Phone: (814) 863-3623. Fax: (814) 863-8403. E-mail: merz@psu.edu.
[†] Universidad de Oviedo.
[‡] The Pennsylvania State University.
[#] On leave from Departamento de Química Física y Analítica, Universidad de Oviedo.

10.1021/jm000340v CCC: $20.00
Published on Web 12/16/2000

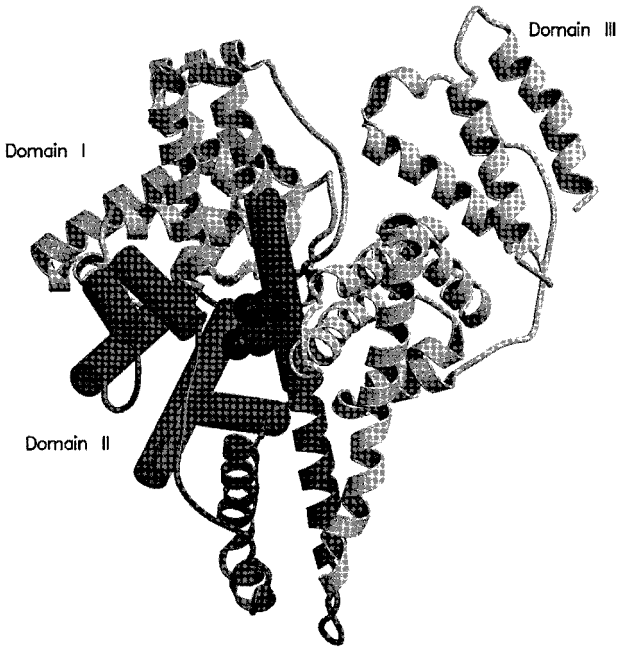

Figure 1. Ribbon model of HSA derived from X-ray crystallography (PDB ID code 1AO6). The α-helices constituting the IIA subdomain are shown as solid cylinders. Lys195 and Lys199 are represented by vdW spheres. This figure was produced with the programs Molscript and Raster3D (refs 34 and 35).

have shown that the principal binding regions are located in subdomains IIA and/or IIIA.[1] The fatty acid molecules bind in long hydrophobic pockets capped by polar side chains, distributed asymmetrically throughout the HSA molecule.[4] The binding of bilirubin, a metabolite of heme and a potent antioxidant in membranes, to HSA has been extensively studied.[1,8] It is now accepted that the high-affinity bilirubin binding site on HSA corresponds to subdomain IIA.[8] The IIA and IIIA binding crevices correspond to the site I and site II regions formerly observed in binding experiments with fluorescence probes.[9] The IIIA binding site appears to possess the primary binding activity for HSA, whereas IIA is more specialized. Both binding sites are structurally characterized by the presence of a buried hydrophobic cavity capped by charged and polar residues.[2,3]

The ability of HSA to covalently bond to different substrates is related to the presence of two highly reactive residues, Lys199 and Tyr411, which are located strategically in the IIA and IIIA binding sites. For example, Lys199 can act as a nucleophile against different IIA ligands. When aspirin binds to the IIA site an esterase reaction occurs and the acetyl group is transferred to the amino group of Lys199.[10] Trinitrobenzenosulfonate and related compounds rapidly transfer the trinitrophenyl group to the amino group of Lys199.[11] The Lys199 and penicillins can also covalently bind via an aminolysis reaction between the β-lactam ring and the ϵ-amino group thereby generating a penicilloyl-containing peptide.[12] Most importantly, these penicilloyl−albumin complexes, which have no antibacterial activity, constitute the major antigenic determinant of penicillin allergy.[13] Penicilloyl groups have also been detected on another five lysine residues of HSA including Lys195. Interestingly, Lys195 is located relatively close to Lys199 in the IIA binding site.[14] Thus, although the primary site of penicilloyl coupling corresponds to the ϵ-amino group of Lys199, the combination of the closely located functional groups of Lys195 and Lys199 could have possible structural and/or mechanistic consequences.

Figure 2 shows a three-dimensional representation of the residues constituting the local environment of Lys199.[5] In the IIA binding site there are a group of hydrophobic residues (Phe211, Leu198, Trp214, Leu219, Leu238, etc.), while the side chains of the hydrophilic residues Gln196, His242, and Tyr150 constitute a polar shell around the Lys199 residue (Tyr150 belongs to the IB subdomain). The key residue, Lys199, is situated in the vicinity of the hydrophobic pocket, its side chain pointing toward the entrance channel of the binding crevice. The other important lysine residue, Lys195, is placed at the opening of the IIA cavity forming a salt bridge with Glu292, which is close to other charged residues such as Arg222, Arg218, etc. Although the resolution of the reported crystal structures of HSA (2.5−2.8 Å) has not allowed a determination of the water content of this binding site, it is reasonable to expect that some water molecules could be associated with the pocket by means of H-bond contacts with the most polar residues.

Clearly, the overall protonation state of Lys195 and Lys199 will determine the mechanism of the chemical reactions between HSA and ligands bound to the IIA site. A central feature of the most likely mechanism(s) requires the ϵ-amino group of the reactive lysine to be deprotonated. This facilitates the nucleophilic attack of this group on electrophilic substrates.[15] Interestingly, the neutral protonation state for Lys199 has been supported by experimental results which show the nonenzymatic reaction of glycosyl and arylating reagents with exceptionally nucleophilic lysine residues such as Lys199. This chemical behavior is consistent with an unusually low pK_a of ∼8 for Lys199 which favors a neutral protonation state.[16]

In this work we report restrained molecular dynamics (MD) simulations of the HSA protein centered on the Nζ atom of Lys199. The influence of positive or neutral configurations of the Lys195 and Lys199 residues on the structural and dynamical properties of the IIA binding site has been addressed by studying three different protonation states. Contacts between functional groups that could be essential elements of the mechanisms for substrate binding and/or chemical reaction may become accessible when the flexibility of the protein is taken into account. These computer simulations have also been valuable in garnering insights into the solvent dynamics and the mechanism of potential proton transfers in the IIA binding site. Particularly, the network of water molecules around the Lys195 and Lys199 residues have been analyzed. Overall, the insights obtained from the MD results could be useful in outlining reaction mechanisms for the formation of protein conjugates involving the Lys195 and Lys199 groups of HSA.

Methods

Three models representing different protonation states of the IIA binding site were set up (see Chart 1). The first model, **L199N**, corresponds to a hypothetical charge distribution of

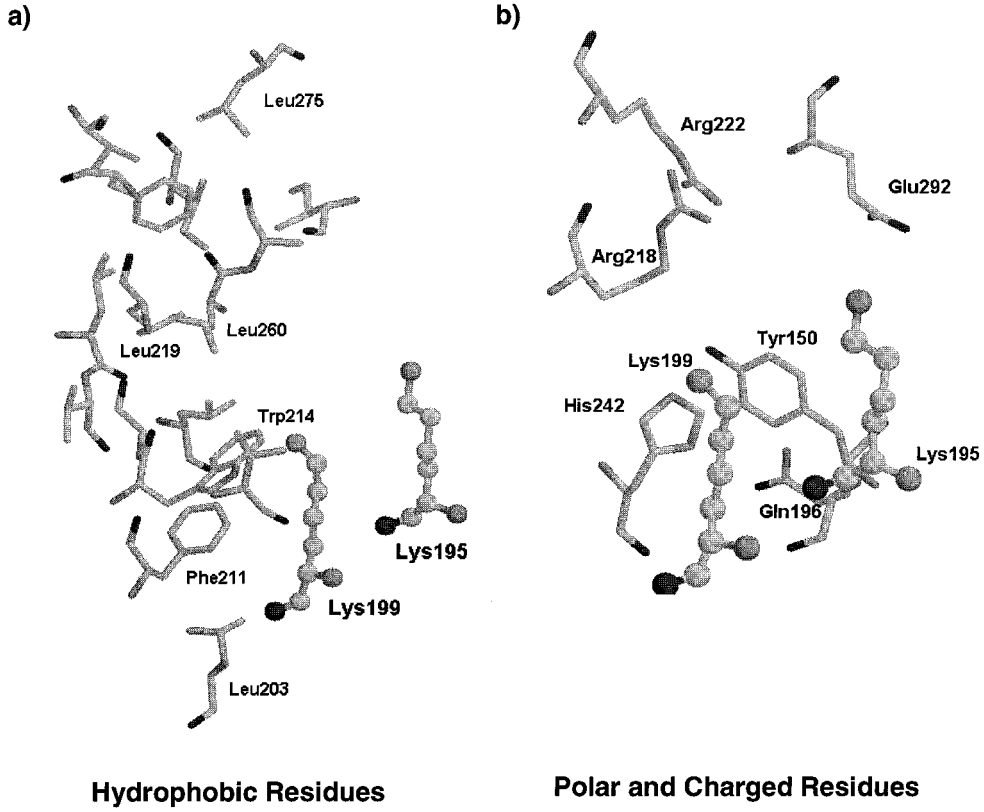

Figure 2. (a) Arrangement of hydrophobic residues in the IIA binding site as derived from X-ray crystallography (PDB ID code 1AO6). (b) Polar residues around the key residue Lys199.

Chart 1

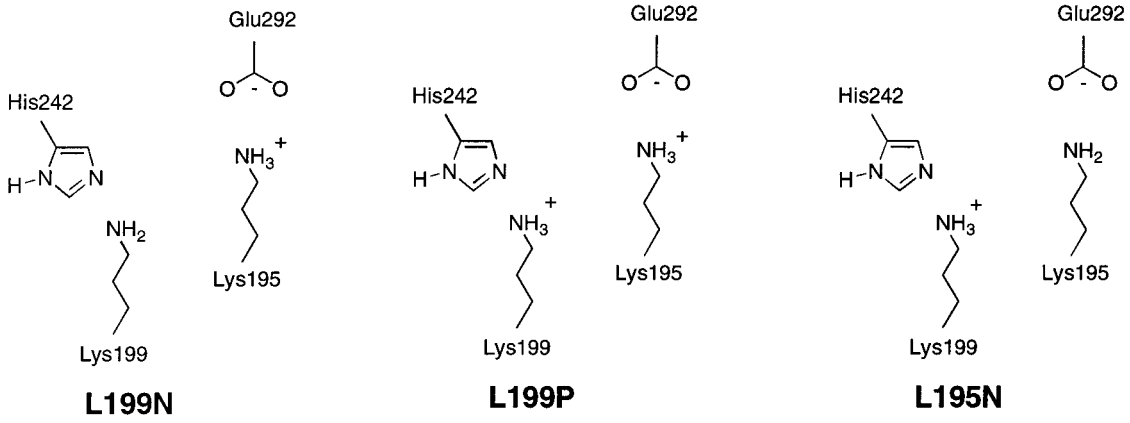

the IIA binding site in which the Lys199 amino group is deprotonated while the charged residues Glu292 and Lys195 form an ionic pair. On the basis of the analysis of the crystallographic structure, His242 was protonated at the δ-position. The **L199N** model seems to be the simplest proposal that agrees with available experimental evidence (see above). The second model examined, **L199P**, is identical to **L199N** except that Lys199 is protonated. In the third model, **L195N**, Lys195 and Lys199 residues are unprotonated and protonated, respectively. The rest of the ionizable residues were set to their pH 7 protonation state. Starting coordinates for all of the models were taken from the HSA molecule A in the 2.5 Å crystal structure of Sugio et al.[5] In addition, water molecules were added within 25 Å of the Nζ@Lys199 atom using the LEAP module[17] of AMBER 5.0.[18] Na^+ counterions were placed by LEAP to neutralize the −15 (**L199P**) and −16 (**L199N, L195N**) charges of the HSA models which arise from the amino acid composition at pH 7. All of the counterions were placed 20 Å beyond the Nζ@Lys199 atom. The resultant model systems contained ∼10 000 atoms.

Energy minimization and MD calculations were carried out using the ROAR 2.0 program[19] with the parm96 version of the all-atom AMBER force field.[20] Removal of bad contacts in the initial geometries was performed using a Limited Memory BFGS minimizer[21] which is included in the latest version of ROAR. Following energy minimization, a 20 Å active zone centered on the Nζ@Lys199 atom was defined, and only residues with at least one heavy atom within this sphere as well as the cap water molecules were allowed to move during the subsequent MD simulations (∼46% of the atoms were moved). The solvent cap was restrained at the 25 Å boundary by a harmonic potential with a force constant of 0.5 kcal/(mol Å).

To ensure the stability of the MD trajectories for these highly charged systems, the time step of the MD simulations was 1.0 fs and the SHAKE algorithm[22] was used to constrain bond lengths at their equilibrium values. A nonbond pairlist cutoff of 15.0 Å was used, and the nonbonded pairlist was updated every 25 time steps. The temperature was maintained at 300 K during the MD simulations using the Nosé−Hoover

chain algorithm for temperature coupling.[23] For both the **L199N** and **L199P** model systems, an equilibration period of 250 ps was followed by a 600-ps production run where coordinates were saved for analyses every 50 time steps. The corresponding MD simulation of the third model, **L195N**, covered 1350 ps because solvent equilibration around Lys195 and Lys199 residues demanded a long equilibration period of 750 ps. During the initial 500 ps of equilibration of **L195N**, the amino and ammonium groups of Lys195 and Lys199, respectively, were interacting directly through a short H-bond. However, the water molecules around Lys195 competed with the ϵ-amino group to form H-bonds with the charged residue Lys199, thereby weakening the Lys195···Lys199 interaction. After solvent equilibration was fully completed, Lys195 and Lys199 acquired clearly defined first-hydration shells, which remained stable for the rest of the simulation. The last 600 ps of the **L195N** trajectory was employed for analysis.

All of the results were analyzed using the Carnal module of AMBER 5.0 and some specific trajectory analysis software developed internally. To estimate the energetics for proton transfer between the Lys195 and Lys199 residues, four different series of QM−MM minimizations[24] were performed in which the Lys195 or Lys199 residue was optimized while the rest of the protein and water environment was held fixed. Initial geometries were taken from snapshots extracted every 2 ps during the **L199N** and **L195N** simulations, resulting in a total of 4 × 300 QM−MM calculations. In these calculations, the PM3 Hamiltonian was used to describe the active lysine residue and the AMBER force field for the MM region. Hydrogen link atoms were placed at the C and N backbone atoms to cap-exposed valence sites due to bonds which cross the QM−MM boundary.[25] The ROAR 2.0 program was also used to carry out the QM−MM calculations.

Results

Root-Mean-Square Deviation and Flexibility of the Subdomain IIA. The active region of HSA, whose conformational space is sampled during the MD simulations, includes nearly all of the residues constituting subdomain IIA as well as some other residues of the rest of the subdomains except those of IIIB. Subdomain IIA comprises six α-helices linked by four disulfide bridges (h1−S−S−h3, h3−S−S−h4, h4−S−S−h5, and h5−S−S−h6) which contribute to stabilize the intradomain structure. Although the definition of domains and subdomains is not rigorous, it is normally accepted that residues within a domain interact more with one another than they do with residues in different domains. Therefore, we expect that the analyses of the MD trajectories from our simulations will be useful to characterize the inherent dynamic properties of subdomain IIA of HSA.

Figure 3 shows the time evolution of the root-mean-squared deviation (rmsd) of the instantaneous structures from the initial crystal structure during the last 600 ps of the MD simulations. These plots indicate that the three models evolve in an equilibrium state with respect to the rms deviations, and they show moderate structural fluctuations which are slightly greater in the **L199N** model. The average rmsd values after equilibration for the protein atoms, the backbone atoms, and the h1−h6 helices in subdomain IIA are given in Table 1. In general, the three models did not deviate significantly from the crystal structure, and their average rmsd values (1.6−2.0 Å) are similar to those observed in other protein simulations. The model **L199P**, in which both Lys195 and Lys199 have a positive charge, gave the lowest rmsd value (1.57 Å total, 1.03 Å backbone), while the **L199N** and **L195N** simulations had greater total

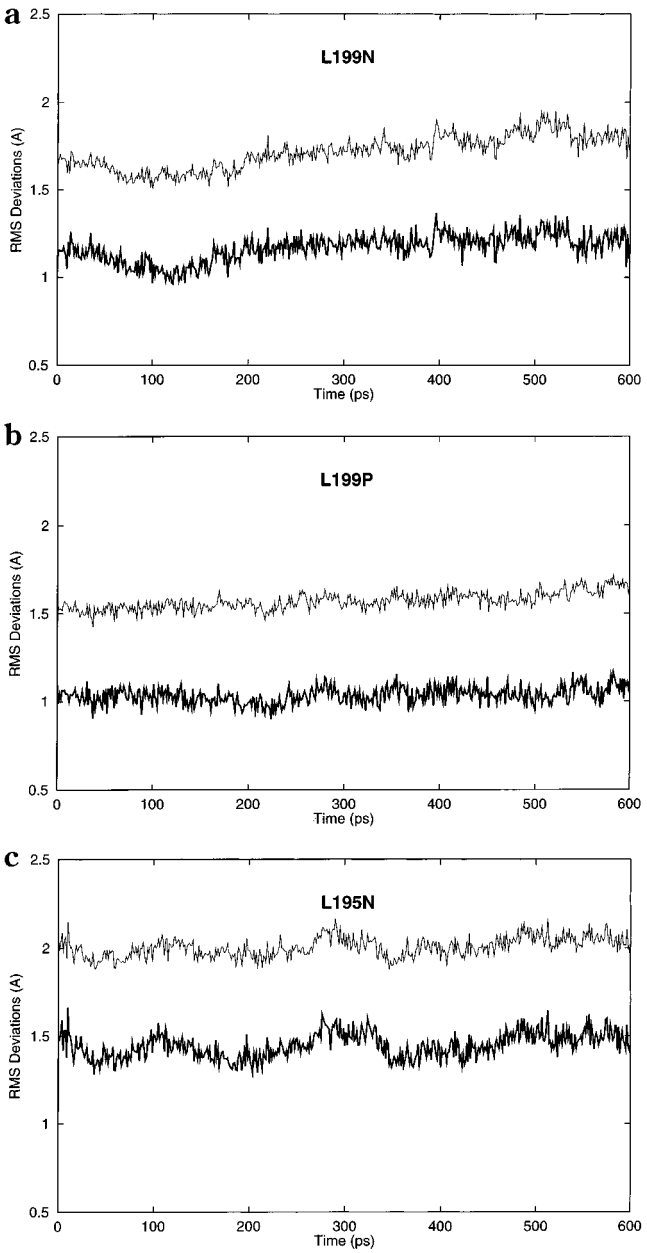

Figure 3. rms Deviation between the instantaneous computed structures and the crystal structure for the IIA subdomain of HSA as a function of time. The bold curve corresponds to the rmsd of the backbone atoms. For the average rmsd values, see Table 1.

rmsd values by 0.15 and 0.43 Å, respectively. A similar trend was observed when the rmsd values were segregated into the h1−h5 helices of the IIA subdomain. This partitioning resulted in rmsd values of 1.0−1.5 Å for the h1−h4 α-helices, whereas h5 had a rmsd value of ∼2.1 Å for the three models (see Table 1). The h5 helix contains only six residues, and its greater deviation with respect to the crystal structure can be well-understood in terms of its solvent exposure. Interestingly, the h6 helix has an unusually high rmsd value of 2.78 Å in the case of the **L195N** trajectory, whereas this small α-helix has much lower rmsd values (1.33 and 1.54 Å) in the **L199N** and **L199P** models (see below).

To gain insight into the fluctuations of subdomain IIA, the rms flexibility (rmsf) was calculated by comparing the instantaneous protein structure to the average one. The rmsf values for the backbone atoms of subdomain

Table 1. Summary of the rmsd and rmsf Values for Subdomain IIA

	L199N	L199P	L195N
	rmsd (Å)		
IIA	1.72 ± 0.10	1.57 ± 0.05	2.00 ± 0.06
IIA backbone	1.17 ± 0.08	1.03 ± 0.05	1.44 ± 0.07
helix h1	1.40 ± 0.14	1.16 ± 0.08	1.26 ± 0.07
helix h2	1.44 ± 0.22	1.09 ± 0.12	1.31 ± 0.11
helix h3	1.10 ± 0.07	1.49 ± 0.06	1.48 ± 0.10
helix h4	1.36 ± 0.13	1.15 ± 0.09	1.33 ± 0.09
helix h5	2.11 ± 0.19	2.05 ± 0.10	2.15 ± 0.13
helix h6	1.33 ± 0.13	1.54 ± 0.18	2.78 ± 0.17
	rmsf (Å)		
IIA	0.75 ± 0.09	0.65 ± 0.04	0.68 ± 0.07
IIA backbone	0.51 ± 0.08	0.43 ± 0.04	0.50 ± 0.06
helix h1	0.60 ± 0.13	0.58 ± 0.08	0.59 ± 0.10
helix h2	0.68 ± 0.10	0.58 ± 0.09	0.54 ± 0.12
helix h3	0.63 ± 0.08	0.54 ± 0.07	0.52 ± 0.08
helix h4	0.64 ± 0.11	0.57 ± 0.08	0.56 ± 0.08
helix h5	0.85 ± 0.29	0.54 ± 0.10	0.66 ± 0.10
helix h6	0.70 ± 0.17	0.75 ± 0.09	0.85 ± 0.13
Tyr150	0.19 ± 0.06	0.18 ± 0.06	0.21 ± 0.08
Lys195	0.46 ± 0.16	0.46 ± 0.18	0.50 ± 0.13
Lys199	0.42 ± 0.10	0.20 ± 0.03	0.29 ± 0.10
Phe211	0.35 ± 0.17	0.14 ± 0.05	0.21 ± 0.11
Trp214	0.20 ± 0.08	0.15 ± 0.05	0.14 ± 0.05
His242	0.19 ± 0.07	0.16 ± 0.06	0.32 ± 0.18
Glu292	0.57 ± 0.08	0.57 ± 0.13	0.57 ± 0.17

IIA are close to the all-atom ones, thereby demonstrating the importance of backbone motion. The rmsf values in Table 1 indicate that, when Lys199 is unprotonated (**L199N** model), subdomain IIA with a rmsf of 0.75 Å is more flexible than in the cases when Lys199 is protonated (**L199P** and **L195N)** which have rmsf values of 0.65 and 0.68 Å, respectively. We also see in Table 1 and Figure 3 that the larger rmsf of the **L199N** model is consistent with the larger fluctuations in its rmsd relative to the crystal structure. It is worth noting that for the three simulations, the larger α-helices (h1−h4) have similar flexibilities of about 0.65 Å (**L199N**), 0.60 Å (**L199P**), and 0.55 Å (**L195N**).

By analyzing the rmsf values of the essential residue Lys199 and other nearby groups (Lys195, His242, Trp214, etc.), we see important changes in the flexibility upon protonation/deprotonation of Lys195 and Lys199. For example, when Lys199 is in its protonated form (**L199P** and **L195N**), the resultant rmsf values (0.20 and 0.29 Å) are clearly lower than that observed in the **L199N** simulation (0.42 Å). On the other hand, Lys195 has a similar flexibility of 0.50 Å in all of the models examined (see Table 1). These changes in the conformational mobility reflect the influence of solvent and/or specific interactions between residues present in each of the simulated protonation states (see below).

Size of the Hydrophobic Pocket. The X-ray structure of HSA identified 16 residues in the h1−h6 α-helices whose hydrophobic side chains constitutes the inside wall of the IIA binding site (see Figure 2a). The relatively large size and approximately ellipsoidal shape of this hydrophobic pocket explain the ability of this binding site to accommodate the hydrophobic part of many classes of substrates. The rmsf values for the side chains of the residues in the hydrophobic pocket obtained from the different trajectories are 0.83 Å (**L199N**), 0.65 Å (**L199P**), and 0.76 Å (**L195N**). According to these rmsf values, the **L199N** simulation yields a hydrophobic pocket which is more flexible than that of **L199P** and **L195N**.

To further estimate the dynamical flexibility and size of the hydrophobic pocket, we also monitored the time evolution of the Cγ@Leu203···Cγ@Leu275 and Cγ@Leu219···Cγ@Leu260 distances (*a, b*). These geometrical parameters were considered as an approximation to the major axes defining the largest ellipsoidal section across this hydrophobic pocket. In all the cases, the average values for *a* and *b* show a reasonable agreement with the corresponding X-ray values (see Table 2 and Figure 2a). The standard deviations of these axes show that the global size and shape of the IIA hydrophobic pocket remain quite stable along the MD trajectories. The **L199N** model presents the largest cavity size although the approximate size of the hydrophobic cavity depends slightly on the protonation state being simulated.

It is interesting to note that the side chains of Phe211 and Trp214, which lie close to Lys199, complex via a $\pi-\pi$ stacking interaction. Because of its position, these residues could significantly contribute to the binding of a hydrophobic part of typical IIA ligands. It has also been proposed that Trp214 plays an important structural role in the formation of the IIA binding site by limiting solvent accessibility.[3] The distance between the center of mass of the corresponding aromatic rings and the angle between the ring planes were examined to characterize the Phe211−Trp214 interaction. We see in Table 2 that the protonation state of Lys199 greatly influences this interaction to the extent that the presence of a positive charge on the Nζ@Lys199 atom reinforces the $\pi-\pi$ stacking interaction by reducing the average distance between the aromatic rings and making them more coplanar. On the other hand, the motion of the aromatic rings is more accentuated in the **L199N** simulation, which could affect binding processes to the IIA site.

Interactions of Lys195 and Lys199 with Other Residues. As discussed in the Introduction, it is well-known that Lys199 is the primary reactive center for HSA via nucleophilic attack on the carbonyl groups of substrates such as aspirin and the penicillins. According to the crystallographic data, the Nζ@Lys199···Nε2@His242 contact has an equilibrium distance of around 4.0 Å, which suggests H-bond interactions. This contact represents the closest interaction between the amino group of Lys199 and its neighbor residues observed experimentally. Hence, it has been proposed that the low pK_a of Lys199 arises from its interaction with the imidazole ring of His242,[2] while for Lys195, the crystal structure clearly suggests the presence of a salt bridge interaction with Glu292 (Nζ@Lys195···Oε@Glu292 distance of ∼3.6 Å). From this structural information, we explored the likely conformations of these residues and their dependence on the protonation state of Lys195 and Lys199.

For the **L199N** trajectory, we found that, in agreement with the X-ray data, the imidazole ring of His242 is stabilized via Nδ1−H···O and Nε2···H−N hydrogen bond contacts with Gln196 and Lys199, respectively (see Table 3 and Figure 4). The average value for the Nδ1@His242···Oδ@Gln196 and Nζ@Lys199···Nε2@His242 distances were 2.9 and 4.3 Å, respectively, while the lifetimes of these hydrogen bonds over the length of the MD trajectories were 99.4% and 40.5%. These values indicate clearly that the interaction between

Table 2. Summary of the rmsf Values (Å) and Significant Distances (Å) between Residues Constituting the Hydrophobic Pocket of the IIA Binding Site

	L199N	**L199P**	**L195N**	X-ray
rmsf[a]	0.68 ± 0.09	0.53 ± 0.07	0.63 ± 0.12	
rmsf (side chain)[a]	0.83 ± 0.12	0.65 ± 0.09	0.76 ± 0.15	
Cγ@Leu203···Cγ@Leu275	25.61 ± 0.82	23.62 ± 0.50	24.58 ± 1.03	23.6
Cγ@Leu219···Cγ@Leu260	7.79 ± 0.38	7.56 ± 0.27	7.60 ± 0.27	9.1
ring@Phe211···ring@Trp214	6.24 ± 0.94	5.35 ± 0.38	6.12 ± 1.26	6.1
angle ring@Phe211···ring@Trp214	31.36 ± 19.82	28.54 ± 11.20	23.99 ± 9.47	27.8

[a] rmsf values for Leu203, Phe211, Trp214, Ala215, Leu219, Phe223, Leu234, Val235, Leu238, Val241, Leu260, Ala261, Ile264, Ile271, Leu275, and Ile290.

Table 3. Summary of Average Distances (Å) between Different Residues of the IIA Binding Site Evaluated from the Three Trajectories

	L199N	**L199P**	**L195N**	X-ray
Nζ@Lys199···Nζ@Lys195	6.73 ± 0.75	8.08 ± 0.59	7.75 ± 0.74	6.9
Nζ@Lys199···Nϵ2@His242	4.26 ± 0.82	3.00 ± 0.17	2.97 ± 0.18	3.7
Nζ@Lys199···Oδ@Gln196	4.60 ± 0.71	2.98 ± 0.20	3.20 ± 0.51	6.3
Nζ@Lys199···ring@Tyr150	6.30 ± 0.57	3.56 ± 0.30	5.06 ± 0.53	7.2
Nδ1@His242···Oδ@Gln196	2.86 ± 0.15	4.44 ± 0.22	5.38 ± 0.35	2.9
Nζ@Lys195···Oϵ1@Glu292	3.80 ± 0.88	4.20 ± 0.96	4.94 ± 1.61	4.8
Nζ@Lys195···Oϵ2@Glu292	3.45 ± 0.83	4.35 ± 1.08	5.94 ± 0.99	3.6

His242 and the amino group of Lys199 is only of moderate strength. Moreover, we observed that the Nζ@Lys199···Nϵ2@His242 distance oscillates with a deviation of ±0.8 Å due to the effect of a competitive interaction between the Nϵ2@His242 atom and the hydroxyl group of the nearby Tyr150 residue. In contrast, the salt bridge between Lys195 and Glu292 is occupied ∼100% during the **L199N** simulation. The Nζ@Lys195···Oϵ@Glu292 salt bridge takes place through a single short N−H···O interaction in which the shortest Nζ···Oϵ distance was 2.5−3.0 Å (the Glu ϵ-oxygen atoms were interchangeable every 100−300 ps of simulation time). The Lys195···Glu292 salt bridge could play an important role in increasing the stability of the entrance channel into the IIA binding site.

The protonation of Lys199 in the **L199P** trajectory significantly affects the nature of the interresidue contacts for this lysine. In this case, the Nδ1@His242··· Oδ@Gln196 contact was lost whereas the interaction between His242 and Lys199 was clearly reinforced as reflected by the computed Nζ@Lys199···Nϵ2@His242 average distance of 3.0 ± 0.2 Å (% occurrence = 99.4%). The strong interaction between His242 and Lys199 could be described as a short, strong H-bond,[26] which is likely favored by the presence of the hydrophobic pocket which results in a local low polarity region around Lys199. A second H-bond between Lys199 and Gln196, which is present in 80% of the **L199P** simulation, contributes to the stabilization of the positive charge on the Nζ@Lys199 atom. The salt bridge between Lys195 and Glu292 was altered since the carboxylate group preferentially forms a bidentate complex with the ammonium group of Lys195 (see average distances in Table 3). Interestingly, the aromatic ring of Tyr150 interacts with the positive charge of Lys199 through a cation−π interaction.[27] The R−NH_3^+ group of Lys199 and the phenol group of Tyr150 form a complex in which the nitrogen atom and the center of mass of the aromatic ring were ∼3.6 ± 0.3 Å (the experimental distance is 7.2 Å) apart (see Figure 4). We note that the stabilization predicted for cation−π complexes, which is normally interpreted to first order as a directional charge−quadrupole attraction, is underestimated by the all-atom AMBER force field.[28] Consequently, it is expected that a cation−π interaction would also be present when the Lys195−Lys199 pair is doubly protonated as in the **L199P** model.

When Lys195 is neutral and Lys199 remains protonated (**L195N** trajectory), we also observed differences with respect to the **L199N** and **L199P** models. The protonated amino group of Lys199 maintains the H-bond interactions with His242 and Gln196 as previously described for the **L199P** simulation. However, this positively charged group interacts weakly through cation−π binding with the aromatic ring of Tyr150 since the average distance from the Nζ atom to the center of mass of the phenol ring (5.1 ± 0.5 Å) is now 1.5 Å greater than that observed for the **L199P** trajectory.

Since Lys195 remains unprotonated in the **L195N** simulation, the link between the h1 and h6 α-helices through the Lys195−Glu292 salt bridge observed in the other model systems disappears. The absence of this structurally important ion pair in the **L195N** trajectory correlates well with its greater rmsd with respect to the crystal structure. This fact can also explain the high rmsd value (2.8 Å) of the nine-residue h6 α-helix. The carboxylate group of Glu292 preserves a weak interaction with the Lys195 amino group, the corresponding Oϵ1···Nζ distance being within typical H-bond distances for 16% of the MD trajectory. The negative charge at Glu292, in this case, is mainly stabilized via interactions with solvent (see below) and with Arg218. No other protein residues form a significant interaction with Lys195.

Solvent Dynamics and Structure. It is well-known that specific interactions between solvent molecules and protein atoms can significantly affect the structure and function of a protein.[29] The reported crystal structures of HSA at 2.5−2.8 Å resolution lack information about the water network in the IIA binding site. Hence, our simulations will provide insights into specific protein−water interactions that are important toward our understanding of substrate binding and chemical reactivity in HSA.

During the simulations, the water molecules located in the IIA binding site hydrate the charged and polar

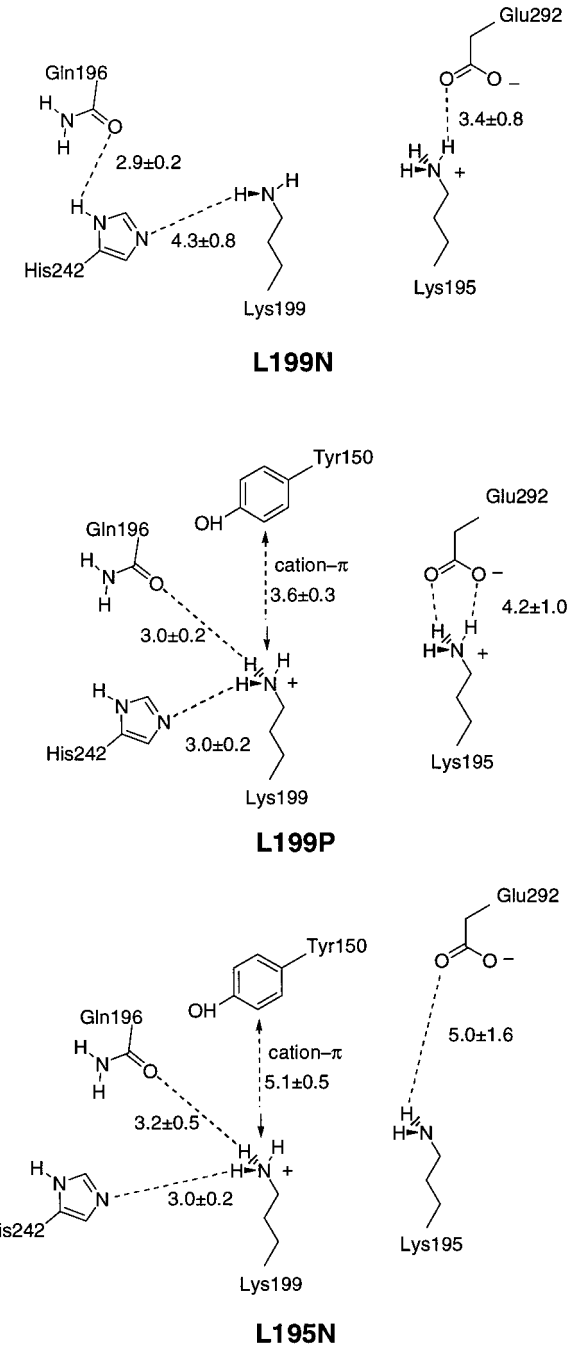

Figure 4. Schematic drawing for the most significant inter-residue contacts found during the **L199N**, **L199P**, and **L195N** simulations. Average distances between heavy atoms and standard deviations are given in Å.

residues (i.e., Lys199, Lys195, Glu292, Tyr150, and His242). We characterized the extent of water penetration and solvent ordering by calculating the pair distribution functions $g(r)$ around the atoms of interest (Nζ@Lys195, Nζ@Lys199, Oϵ@Glu292, etc.; see Table 4). In addition, we studied the nature of the water bridges[30] connecting the amino groups of Lys195 and Lys199. In this case, a solvent H-bond is considered to be present if both distance (e.g., O−O < 3.5 Å) and angular (e.g., O−H···O > 120°) criteria are satisfied simultaneously.

For the **L199N** trajectory, the $g(r)$ function for both Nζ atoms of Lys195 and Lys199 shows sharp peaks at 2.90 and 2.87 Å, which show a stable first solvation sphere around these groups. Integration of the $g(r)$ plot out to the first minimum at ∼3.8 Å indicates that there are four and two water molecules in the first solvation layers for Lys195 and Lys199, respectively. The coordination number for Lys199 is one-half of that typically found for charged residues, which are solvent-exposed (4−5). This is because Lys199 is located adjacent to a hydrophobic pocket in the IIA binding site of HSA. The $g(r)$ functions centered on the Oϵ1 and Oϵ2 atoms of Glu292 have a first peak at 2.7 Å with integrated values of 1.7 and 1.5 Å, respectively. This reflects the strength of the Nζ@Lys195···Oϵ@Glu292 salt bridge, which is maintained through a single H-bond interaction. His242 and Tyr150 show low intensity peaks at 2.9 Å around their Nϵ2 and Oη atoms, respectively. The integration of these peaks give values of 1.1 and 0.5 Å, respectively, thereby showing the presence of at least one long-lived "deep" water hydrating these residues.

Table 4. First Peak Position (Å) of the Atomic Radial Distribution Function $g(r)$[a]

atom	L199N	L199P	L195N
Nζ@Lys199	2.87 (1.96)	2.89 (1.84)	2.88 (2.67)
Nζ@Lys195	2.90 (4.39)	2.90 (5.07)	2.91 (4.11)
Oϵ1@Glu292	2.67 (1.69)	2.68 (3.19)	2.66 (3.13)
Oϵ2@Glu292	2.68 (1.50)	2.67 (3.56)	2.66 (2.53)
Nϵ2@His242	2.92 (1.10)	5.58 (2.06)	4.08 (1.30)
Oη@Tyr150	2.92 (0.50)	2.84 (0.62)	2.88 (0.80)

[a] Integrated values of $g(r)$ until the first minimum are in parentheses.

Interestingly, some of the water molecules hydrating the Nζ atoms establish a fluxional network of hydrogen bonds which connects the protonated (Lys195) and deprotonated (Lys199) amino groups during the **L199N** simulation. The possible water bridges between these groups can be categorized as sequential hydrogen bonding, $N_\zeta-H\cdots(H_2O)_n\cdots N\zeta$, and double-acceptor hydrogen bonding, $N\zeta-H\cdots(H_2O)_n\cdots H-N\zeta$. We found that the sequential networks were observed in 90.2% of the analyzed snapshots while the percentage of occurrence of double-acceptor H-bond networks is only 36.3%.

Figure 5 presents sequential water bridges from Lys199 to Lys195 involving two, three, and four water molecules. The number of bridging water molecules and the average distances between the donor−acceptor atoms indicate that the second hydration shells of Lys195 and Lys199 overlap to form the organized cluster of H-bonds connecting the donor (Nζ@Lys199) and acceptor (Nζ@Lys195) ends. It should be noted that the water bridges in Figure 5 are *linear* in terms of graph theory terminology.[31] For the **L199N** simulation, the majority of linear water bridges consisted of three water molecules (47.5% of snapshots). The two- and four-water-molecule bridges are also quite favorable (34.0 and 23.0%, respectively) while the extreme cases of one- and five-water-molecule bridges are much less likely (4.1 and 5.4%, respectively). We also note that other *branched* water bridges normally coexist with the linear ones.

As expected the water bridges were observed to undergo fast rotational motions (i.e., exchange of the H-bonds from water atom H1 to H2 (and vice versa)). Simultaneously, other water molecules diffuse in and/or replace existing water molecules in the bridge. Thus, the calculated lifetimes for the most common water

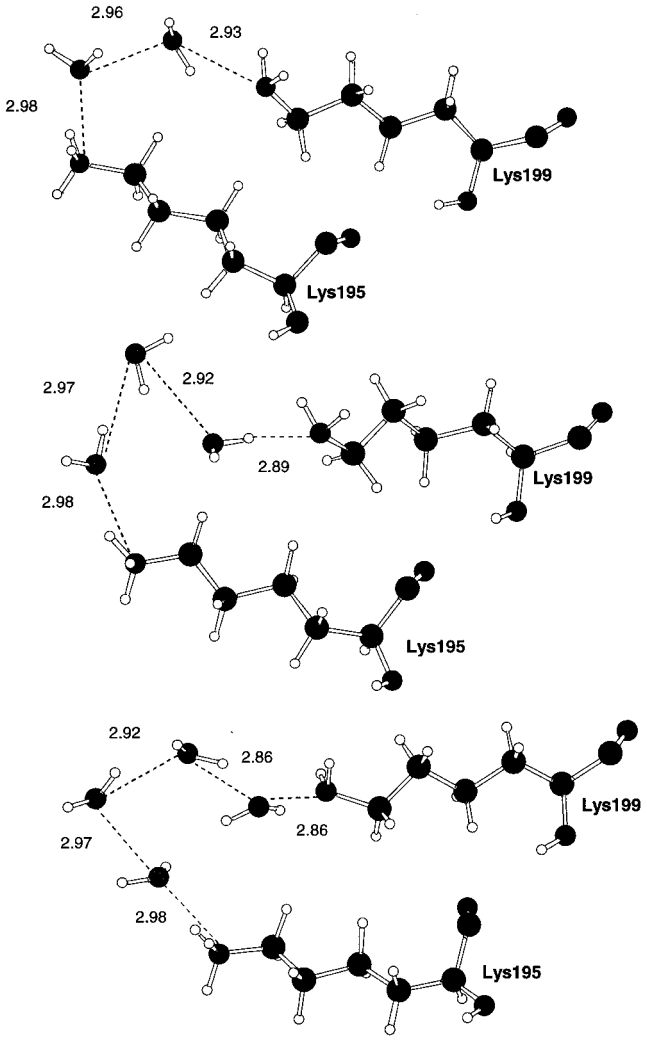

Figure 5. Arrangement of sequential H-bonding water bridges connecting the Lys195 and Lys199 residues at specific snapshots taken from the **L199N** trajectory. Distances between heavy atoms (Å) were obtained by averaging the geometry of the two-, three-, and four-water-molecule bridges along the entire **L199N** trajectory.

bridges were quite short, ranging from 0.2 to 7 ps. Nevertheless, we stress that the *total* (i.e., independent of the water bridge length) probability of water bridge formation along the **L199N** simulation remains very high (90.2%). Therefore, it is clear that the bridging water molecules play a fundamental role in stabilizing the orientation of Lys195 and Lys199 in the **L199N** model.

The number of sequential hydrogen networks from Nζ@199 to Nζ@195 formed exclusively by donor → acceptor H-bonds was large (as opposed to double-acceptor hydrogen bond patterns). Indeed the percentage of the three- and two-water-molecule bridges, which correspond to fully donor → acceptor H-bond bridges, is 54.5 and 75.5%, respectively (29.4 and 28.0% in terms of the number of snapshots). Overall, these results strongly suggest that the solvent positioning and dynamics are adequate enough to promote proton-transfer processes from the protonated Lys195 amino group to the neutral Lys199 residue.

For the **L199P** simulation, the $g(r)$ functions for the Nζ atoms were similar to those for the **L199N** case (see Table 4). The previously described weakness in the Lys195−Glu292 salt bridge during the **L199P** trajectory can be correlated with the coordination number around the Oϵ atoms of Glu292 (3 water molecules) compared with that observed in the **L199N** simulation (∼1 water molecule). Similarly, the strong interaction between Lys199 and His242 is reflected in the absence of a first hydration layer around the Nϵ2 atom of the histidine residue (see Table 4). We also characterized the presence of double-acceptor hydrogen bonding networks connecting the charged Lys195 and Lys199. In this case, the population of the three- and two-water-molecule linear bridges amounts to 52.8 and 28.8%, respectively. Thus, solvent also plays an important structural role in stabilizing the configuration of these lysine positive groups through the occurrence of organized H-bonds.[29]

For the third simulation (**L195N**), which is formally connected with **L199N** through a Lys199 → Lys195 proton transfer, the observed solvent structure and dynamics present unusual features. While the first solvation layer of the Nζ atom of Lys195 contains four water molecules as in the **L199N** simulation, the average number of water molecules around the positively charged Lys199 residue increases from 1.96 to 2.67. This can be interpreted in terms of an extra water molecule located in the region of the hydrophobic pocket. The hydration of His242 and Tyr150 is similar to that described for the **L199P** simulation. Important changes were revealed by the analysis of the water bridges which link the acidic (Lys199) and basic (Lys195) groups. Although the mean Nζ@Lys199···Nζ@Lys195 separation increases by ∼1.0 Å (see Table 3), the total abundance of sequential hydrogen bonding networks was substantially lowered when a proton was transferred from Lys195 to Lys199. During the **L195N** simulation, there were 45.5% snapshots showing water bridges compared with the 90.2% value observed for the **L199N** simulation. Also the number of water molecules in the water bridges was greater as reflected by the population of *linear* water bridges of three (9.6% of snapshots), four (14.9%), and five (20.1%) water molecules. As expected, the probability of fully donor → acceptor water bridges decreases as the mean length of the water bridges increases. We observed that the snapshots containing three-, four-, and five-water-molecule bridges with a fully donor → acceptor character are only 5.8, 2.7, and 1.4% of the total snapshots, respectively. These changes in the water networks could determine both the probability and the mechanism of proton transfer from Lys199 to Lys195.

Energetic Analysis of Proton Transfer between Lys195 and Lys199. To further compliment the geometrical analyses of protein−protein and solvent−protein interactions, we performed a series of QM−MM calculations in which Lys195 or Lys199 was described at the PM3 semiempirical level. The QM−MM energy minimizations of these residues gave their average PM3 heats of formation. These enthalpy terms, which include the environmental effects of the rest of the protein residues and solvent molecules, are probably better described as solvation enthalpies.[32]

To roughly estimate the relative stability of the **L199N** and **L195N** models, we considered the enthalpy change of the corresponding proton-exchange process as expressed by the following relationship:

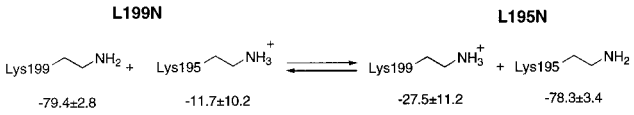

where the indicated average heats of formation (kcal/mol) were computed separately for each residue as described in the Methods section. The global enthalpy change, which is obtained by subtracting the mean values, is −14.7 kcal/mol favoring the **L195N** state. This energy difference is relatively small since it has a magnitude similar to the fluctuations of the individual energy terms for the charged residues. Therefore, from this energetic analysis, we conclude that, in terms of the intrinsic basicity of Lys195 and Lys199, the **L199N** and **L195N** protonation states are close in energy. We also note that entropic contributions could well-favor the **L199N** model due to its larger flexibility. Therefore, it may be reasonable to expect that both states are energetically accessible and could be rapidly interconverting through H-bond rearrangements and proton-exchange processes.

Discussion

Comparison with the X-ray Structure. On the basis of the differences observed in the rmsd values corresponding to the three trajectories, the actual protonation state of the Lys195−Lys199 pair in the native structure of the IIA binding site of HSA cannot be clearly delineated. However, a comparative analysis of the most important residue−residue contacts observed in our MD simulations with those determined crystallographically could give some insight into which model system (**L199N**, **L199P**, or **L195N**) is most likely to represent the IIA binding site.

With respect to the crystal structure of the IIA subdomain, the largest total rmsd (∼2.0 Å) and the largest rmsd of a single α-helix (2.8 Å for h6) were observed in the **L195N** trajectory in which Lys195 and Lys199 were described as neutral and positively charged residues, respectively. As previously mentioned, this observation appears to be a consequence of the absence of the Lys195−Glu292 salt bridge in this simulation. This salt bridge, which is clearly present in the crystallographic configuration of HSA linking the h1 and h6 α-helices of the IIA subdomain, is probably an important element in stabilizing the intradomain structure of this region of HSA. From this structural deficiency, it is reasonable to conclude that the **L195N** model is not a good model for the X-ray structure of HSA.

The MD trajectories calculated for **L199N** and **L199P**, which differ only in the protonation state of Lys199, gave similar rmsd values for the IIA subdomain and for specific α-helices (see Table 1). When Lys195 and Lys199 were protonated (**L199P**), we noted that the residue−residue contacts of both lysines were stable. While Lys195 maintains a salt bridge interaction with Glu292, which is in agreement with experimental data, the stabilization of Lys199 via *short* H-bonds with His242 and Gln196 and a cation−π interaction with Tyr150 is not so compatible with experimental observation. Particularly, the absence of the cation−π interaction in the experimental structure suggests that the **L199P** model can be discarded as an appropriate theoretical model for the IIA binding site. On the other hand, Lys199 as a neutral residue (**L199N**) preserves the main residue−residue contacts observed experimentally and results in average distances for the most significant contacts which are in good agreement with those obtained from the X-ray coordinates (see Table 3). Thus, by comparison with the crystallographic coordinates, our simulations suggest that the actual protonation state of the IIA binding site corresponds to that of the **L199N** model.

Other dynamical and structural aspects further support **L199N** as an accurate theoretical model for the IIA binding site. As discussed above, for the **L199N** model, the flexibility of the side chains of the residues constituting the IIA hydrophobic pocket is clearly greater than that observed in the **L199P** and **L195N** simulations. In particular, two important aromatic residues located at the entrance of the hydrophobic pocket, Phe211 and Trp214, are more flexible when Lys199 is deprotonated and, therefore, potentially more suited to binding the hydrophobic tail of substrate molecules. Thus, the **L199N** model could facilitate the entrance and exit of a broader spectrum of ligands due to the larger structural fluctuations of its hydrophobic pocket.

Chemical Reactivity of Lys199. As discussed in the Introduction, Lys199 is thought to be a highly reactive residue capable of attacking different IIA ligands through nucleophilic substitution processes. The ability of Lys199 to react with glycosyl and arylating agents as well as with acetyl salicylate and penicillins is consistent with a pK_a of ∼8 for Lys199. Our results add theoretical support to these proposals because, besides comparing favorably with the X-ray structure, the **L199N** model is clearly in agreement with the observed chemical reactivity of Lys199. Moreover, the neutral protonation state of Lys199 results in a greater conformational mobility that might favor the formation of a prereactive HSA−substrate complex.

On the basis of the crystallographic data,[2,3] the origin of the low pK_a for Lys199 has been ascribed to its interaction with His242. However, the simulation **L199N** demonstrates that the Nζ@Lys199···Nϵ2@His242 interaction is only of moderate strength, which seems insufficient to explain the pK_a shift of Lys199. To further understand this point, we examined the distribution of charged residues around Lys199 for distances between 6 and 14 Å, which could influence the pK_a through long-range electrostatic interactions.[33] We see in Table 5 that numerous charged groups surround Lys199, the average separation between Lys199 and positively charged residues (Lys195, Arg218, Arg222, Arg197, and Arg257) being slightly lower than that for the negative ones (Glu292, Asp251, Glu153, Glu244, etc.). Furthermore, all of the anionic groups are located on the protein surface (i.e., in environments that resemble bulk solvent), whereas only two arginine residues, Arg218 and Arg222, are partially solvent-exposed while the remaining arginines are buried in the hydrophobic core of HSA. This asymmetric distribution of negatively and positively charged residues is in agreement with the affinity of the IIA binding site for hydrophobic anionic substrates of small size. Moreover, the local accumulation of relatively buried positive charges around Lys199 could well-disfavor its protonated configuration thereby

Table 5. Summary of the Average Distances (Å) and Standard Deviations from Selected Charged Residues to the Nζ@Lys199 Atom during the **L199N** Simulation

atom	distance positive residues	atom	distance negative residues
Nζ@Lys195	6.73 ± 0.75	Cδ@Glu292	9.72 ± 0.69
Cζ@Arg218	9.31 ± 0.62	Oε1@Glu292	9.88 ± 1.20
Nη1@Arg218	9.07 ± 0.69	Oε2@Glu292	9.53 ± 1.18
Nη2@Arg218	10.58 ± 0.62	Cγ@Asp251	9.12 ± 0.94
Cζ@Arg222	9.98 ± 0.89	Oδ1@Asp251	9.08 ± 1.40
Nη1@Arg222	9.12 ± 0.83	Oδ2@Asp251	8.63 ± 1.04
Nη2@Arg222	9.86 ± 1.30	Cδ@Glu153	10.20 ± 0.62
Cζ@Arg197	13.05 ± 0.66	Oε1@Glu153	10.80 ± 0.66
Nη1@Arg197	12.70 ± 0.69	Oε2@Glu153	10.64 ± 0.71
Nη2@Arg197	14.34 ± 0.67	Cδ@Glu244	13.83 ± 0.61
Cζ@Arg257	10.11 ± 0.77	Oε1@Glu244	13.26 ± 0.64
Nη1@Arg257	10.98 ± 0.90	Oε2@Glu244	14.91 ± 0.67
Nη2@Arg257	9.56 ± 0.79	Cδ@Glu188	12.64 ± 0.53
		Oε1@Glu188	12.04 ± 0.58
		Oε2@Glu188	13.61 ± 0.66

explaining its lower pK_a. Further computational work seems necessary to validate this interpretation.

Chemical Reactivity of Lys195. The characterization of the structure and dynamics of the water molecules around Lys195 and Lys199 gives some insight into the influence of solvent on the different models **L199N**, **L199P**, and **L195N**. For the preferred **L199N** model, our analyses demonstrate that the probability of the basic form of Lys199 being connected to the acid form of Lys195 through a network of H-bonding water molecules is very high. Moreover, this water-mediated link between lysine residues is dominated by three- and two-water-molecule bridges with a donor → acceptor character. On the one hand, these water bridges could play an important structural role in stabilizing the **L199N** configuration. On the other hand, it might be expected that the solvent organization present in the **L199N** model could facilitate a Lys195 → Lys199 proton transfer. Moreover, because the two amino groups are of similar basicity, the intrinsic energy barrier for proton transfer could be low and tunneling could play a role in the reaction. These results qualitatively suggest that the **L199N** → **L195N** interconversion might be possible.

By estimating the heat of formation of the Lys195−Lys199 pair influenced by the **L199N** and **L195N** environments, the reaction energy for this pair of residues upon proton exchange was found to be low and of a similar magnitude to the fluctuations in the computed energy. Of course, it should be taken into account that this energy change is only a contribution to the *total* energetics of the **L199N** → **L195N** interconversion. For example, the loss of the Glu292−Lys195 ionic pair may disfavor the **L195N** configuration energetically. Hence, obtaining a quantitative picture of this proton transfer will require the inclusion of long-range effects and the calculation of the total free energy change associated with this process. Nonetheless, these preliminary results indicate that the **L199N** → **L195N** interconversion is likely not to be strongly disfavored.

The proton-transfer process converting **L199N** into **L195N** could be an explanation for the ability of Lys195 to react with penicillins and other reagents.[13] Our simulations suggest that the acid−base pair formed by the amino groups of Lys195 and Lys199 could be a major feature of the structure and dynamics of the IIA binding site. If these residues could undergo proton interchange readily, it would be expected that both lysines could act as nucleophiles as experimentally observed in the case of penicillin binding to HSA. Nevertheless, the amino group of Lys199 is closer to the hydrophobic pocket and less solvent-exposed than that of Lys195; therefore, Lys199 should react more efficiently against the hydrophobic organic anions typically bound by the IIA binding site.

Implications for Bilirubin Binding to HSA. Very recently, site-directed mutagenesis studies of HSA (K195M, K199M, F211V, W214L, R218M, R222M, H242V, and R257M) have been used to study the role of various amino acid residues in the binding of bilirubin.[8] Quite surprisingly, these studies showed that the mutation of certain positively charged and aromatic residues do not alter the affinity of HSA for bilirubin. The authors have proposed that HSA has an unusually high degree of flexibility that results in a situation in which no single residue is critical in providing the free energy of binding for bilirubin. However, previous thermodynamic work on the bilirubin−HSA interaction has shown that the negative $\Delta G_{binding}$ (−11.0 kcal/mol) is mainly provided by a enthalpy change (−13.5 kcal/mol).[1] These data have been interpreted in terms of the predominance of electrostatic interactions between the two carboxylate groups of bilirubin and key lysine or arginine residues rather than hydrophobic forces between bilirubin and nonpolar residues in the binding pocket.

The results of our MD simulations are useful in further understanding why HSA mutants do not have a strong effect on the affinity of HSA for bilirubin. Assuming that the **L199N** model represents the structure of wild-type HSA, the mutation of the *neutral* Lys199 residue into Met199 would not change the global charge of the IIA binding site. Similarly, the mutation of charged residues such as Lys195, Arg222, etc., could also preserve the global charge of the binding site. This would occur if the electrostatic effect of these mutations (charged to neutral) would shift the pK_a of Lys199 higher, which would then protonate Lys199 at physiological pH and retain the overall charge of the active site. Thus, the conservation of the global positive charge in all of the mutant species studied experimentally could facilitate the binding of bilirubin by short- and long-range electrostatic interactions.

Conclusions

The MD simulations of the IIA binding site of HSA reported herein have given us insights into the preferred residue−residue contacts and solvent structure around the highly reactive residues Lys195 and Lys199. Through a comparison of the X-ray coordinates with our simulated models for the Lys195−Lys199 pair, we conclude that the **L199N** (Lys195 and Lys199 were protonated and neutral, respectively) model is preferred. **L199N** was selected because it explains the experimentally observed residue−residue contacts and is also in agreement with the proposed low pK_a value for Lys199. In this model, the water molecules around the active lysine residues define a water bridge that might be important for stabilizing the **L199N** configuration. It could also facilitate a proton transfer between Lys195 and Lys199, which leads to the **L195N** state. Although the lack of

the Lys195−Glu292 ion pair eliminates **L195N** as a representative model for the X-ray structure of HSA, our simulations suggest that a configuration with Lys195 in its basic (nucleophilic) form cannot be definitively discarded. The **L199N → L195N** interconversion might explain the reported nucleophilic ability of Lys195 against penicillin derivatives that are typical substrates for the IIA binding site. Therefore, both lysine residues located in the IIA binding site of HSA, Lys195 and Lys199, could play a combined and comparable chemical role.

Acknowledgment. We thank the NIH for support of this work via Grant GM44974. We also thank the National Center for Supercomputer Applications (NCSA) for generous allocations of supercomputer time. N.D., D.S., and T.L.S. are grateful to MEC (Spain) for partial financial support of this work (PB97-1300). N.D. and D.S. also thank MEC for their Grants PB98-44430549 and EX99-10863995Z, respectively.

References

(1) Peters, T. *All about Albumin: Biochemistry, Genetics and Medical Applications*; Academic Press: San Diego, CA, 1996.
(2) Carter, D. C.; Ho, J. X. Structure of Serum Albumin. *Adv. Protein Chem.* **1994**, *45*, 153−203.
(3) He, X. M.; Carter, D. C. Atomic Structure and Chemistry of Human Serum Albumin. *Nature* **1992**, *358*, 209−215.
(4) Sugio, S.; Mochizuki, S.; Noda, M.; Kashima, A. Crystal Structure of Human Serum Albumin at 2.5 Å. *Protein Eng.* **1999**, *12*, 439−446.
(5) Curry, S.; Mandeikow, H.; Brick, P.; Franks, N. Crystal Structure of Human Serum Albumin complexed Fatty Acids reveals an Asymmetric Distribution of Binding Sites. *Nat. Struct. Biol.* **1998**, *5*, 827−835.
(6) Dockal, M.; Carter, D. C.; Rüker, F. The three recombinant domains of human serum albumin − Structural characterization and ligand binding properties. *J. Biol. Chem.* **1999**, *274*, 29303−29310.
(7) Landau, M. Molecular Mechanisms of Interactions of Physiologically Active Molecules with Biopolymers and Biomembranes (Physicochemical Studies). *Russ. J. Org. Chem.* **1998**, *34*, 615−628.
(8) Petersen, C. E.; Ha, C. E.; Harohalli, K.; Feix, J. B.; Bhagavan, N. V. A Dynamic Model for Bilirubin Binding to HSA. *J. Biol. Chem.* **2000,** *275*, 20985−20995.
(9) Sudlow, G.; Birkett, D. J.; Wade, D. N. Further characterization of specific drug binding sites on HSA. *Mol. Pharmacol.* **1976**, *12*, 1052−1061.
(10) Gerig, J. T.; Katz, R. E.; Reinheimer, J. D., Sullivan, G. R.; Roberts, J. D. Examination of the aspirin acetylation site of HSA by 13C NMR spectroscopy. *Org. Magn. Reson.* **1981**, *15*, 158−161.
(11) Kurono, Y.; Ichioka, K.; Ikeda, K. Kinetics of the rapid Modification of HSA with Trinitrobenzenesulfonate and Localization of its site. *J. Pharm. Sci.* **1983**, *72*, 432−435.
(12) Yvon, M.; Anglade, P.; Val. J. M. Identification of Lysine Residue 199 of Human Serum Albumin as a Binding Site for Benzylpenicilloyl Groups. *FEBS Lett.* **1988**, *239*, 237−240.
(13) (a) Levine, B. B.; Ovary, Z. Studies en the Mechanism of the Formation of the Penicillin Antigen III. The N-(D-α-Benzylpenicilloyl) Group as an Antigenic Determinant Responsible for Hypersensitivity to Penicillin D. *J. Exp. Med.* **1961**, *114*, 875−904. (b) Saxon, A.; Beall, G. N.; Rohr, A. S.; Adelman, D. C. Immediate Hypersensitivity Reactions to β-Lactam Antibiotics. *Ann. Int. Med.* **1987**, *107*, 204−215.
(14) (a) Yvon, M.; Anglade, P.; Val. J. M. Binding of Benzyl Penicilloyl to Human Serum Albumin. Evidence for a Highly Reactive Region at the Junction of Domains 1 and 2 of the Albumin Molecule. *FEBS Lett.* **1989**, *247*, 273−278. (b) Yvon, M.; Anglade, P.; Val. J. M. Identification of the Binding Sites of Benzyl Penicilloyl, the Allergenic Metabolite of Penicillin, on the Serum Albumin Molecule. *FEBS Lett.* **1990**, *263*, 237−240.
(15) Díaz, N.; Suárez, D.; Sordo. T. L. Theoretical Study of Water-Assisted Aminolysis of β-lactams: Implications for the Reaction between Human Serum Albumins and Penicillins. *J. Am. Chem. Soc.* **2000**, *122*, 6710−6719.
(16) (a) Gerig, J. T.; Reinheimer, J. D. Modification of HSA with trifluoromethyl-substituted Aryl Halides and Sulfonates. *J. Am. Chem. Soc.* **1975**, *97*, 168−173. (b) Gerig, J. T., Katz, K. E., Reinheimer, J. D. Reactions of 2,6-dinitro-4-trifluoromethylbenzenesulfonate with HSA. *Biochim. Biophys. Acta* **1978**, *534*, 196−209.
(17) Schafmeister, C.; Ross, W. S.; Romanovski, V. *LEAP*; University of California: San Francisco, 1995.
(18) Case, D. A.; Pearlman, D. A.; Caldwell, J. W.; Cheatham II, T. E.; Ross, W. S.; Simmerling, C. L.; Darden, T. A.; Merz, K. M.; Stanton, R. V.; Cheng, A. L.; Vincent, J. J.; Crowley, M.; Ferguson, D. M.; Radmer, R. J.; Seibel, G. L.; Singh, U. C., Weiner. P. K.; Kollman, P. A. *AMBER5*; University of California: San Francisco, 1997.
(19) Cheng, A.; Stanton, R. S.; Vincent, J. J.; van der Vaart, A.; Damodaran, K. V.; Dixon, S. L.; Hartsough, D.S.; Mori, M. Best, S. A.; Monard, G.; Garcia, M.; Van Zant, L. C.; Merz, K. M., Jr. *ROAR 2.0;* The Pennsylvania State University: University Park, 1999.
(20) Cornell, W. D.; Cieplak, P.; Bayly, C. I.; Gould, I. R.; Merz, K. M., Jr.; Ferguson, D. M.; Spellmeyer, D. C.; Fox, T.; Caldwell, J. W.; Kollman, P. A. A Second Generation Force Field for the Simulation of Proteins, Nucleic Acids, and Organic Molecules. *J. Am. Chem. Soc.* **1995**, *117*, 5179−5197.
(21) Liu, D. C.; Nocedal, J. On the Limited Memory BFGS method for large scale optimizations. *Math. Program.* **1989**, *45*, 503−528.
(22) Van Gunsteren, W. F.; Berendsen, H. J. C. Algorithm for macromolecular Dynamics and Constraint Dynamics. *Mol. Phys.* **1977**, *34*, 1311.
(23) Cheng, A.; Merz, K. M., Jr. Application of the Nose-Hoover Chain Method to the Study of Protein Dynamics. *J. Phys. Chem.* **1996**, *100*, 1927−1937.
(24) Monard, G.; Merz, K. M., Jr. Combined Quantum Mechanical/Molecular Mechanical Methodologies Applied to Biomolecular Systems. *Acc. Chem. Res.* **1999**, *32*, 904−911.
(25) Field, M. J., Bash, P. A.; Karplus. M. A Combined QM and MM potential for MD simulations. *J. Comput. Chem.* **1990**, *11*, 700−773.
(26) Gerlt, J. A.; Kreevoy, M. M.; Cleland, W. W.; Frey, P. A. Understanding enzymatic catalysis: The importance of short, strong hydrogen bonds. *Chem. Biol.* **1997**, 4, 259−267.
(27) Ma, J. C.; Dougherty, D. A. The π-Cation Interaction. *Chem. Rev.* **1997**, *97*, 1303−1324.
(28) Chipot, C.; Maigret, B.; Pearlman, D. A.; Kollman, P. A. Molecular Dynamics Potential of Mean Force Calculations: A Study of the Toluene−Ammonium−Cation Interactions. *J. Am. Chem. Soc.* **1996**, *118*, 2998−3005.
(29) Brooks, C. L., III; Karplus, M.; Pettitt, B. M. In *Proteins. A Theoretical Perspective of Dynamics, Structure and Thermodynamics*; Prigogine, I., Rice, S. A., Eds.; John Wiley & Sons: New York, 1988; Advances in Chemical Physics Vol. LXXI.
(30) Toba, S.; Colombo, G.; Merz, K. M., Jr. Solvent Dynamics and Mechanism of Proton Transfer in Human Carbonic Anhydrase II. *J. Am. Chem. Soc.* **1999**, *121*, 2290−2302.
(31) Trinajstic, N. *Chemical Graph Theory*; CRC Press: Boca Raton, FL, 1992.
(32) Merz, K. M.; Banci, L. Binding of Azide to HCAII: The Role Electrostatic Complementary Plays in Selecting the Preferred Resonance Structure of Azide. *J. Phys. Chem.* **1996**, *100*, 17414−17420.
(33) Antonsiewicz, J.; McCammon, J. A.; Gilson, M. K. The Determinants of pK_as in Proteins. *Biochemistry* **1996**, *35*, 7819−7833.
(34) Kraulis, P. J. Molscript: A Program to Produce both Detailed and Schematic Plots of Protein Structures. *J. Appl. Crystallogr.* **1991**, *24*, 946−950.
(35) Merritt, E. A.; Bacon, D. J. Raster3D: Photorealistic Molecular Graphics. *Methods Enzymol.* **1997**, *277*, 505−524.

JM000340V